THE JOURNAL OF BIOLOGICAL CHEMISTRY VOL. 288, NO. 43, pp. 30904–30916, October 25, 2013

Protection of a Ceramide Synthase 2 Null Mouse from Drug-induced Liver Injury

ROLE OF GAP JUNCTION DYSFUNCTION AND CONNEXIN 32 MISLOCALIZATION[*S]

Received for publication, August 28, 2013, and in revised form, September 8, 2013 Published, JBC Papers in Press, September 9, 2013, DOI 10.1074/jbc.M112.448852

Woo-Jae Park[‡§1], Joo-Won Park[‡¶1], Racheli Erez-Roman[‡2], Aviram Kogot-Levin[‡‖], Jessica R. Bame[**], Boaz Tirosh[‡‡], Ann Saada[‖], Alfred H. Merrill, Jr.[**], Yael Pewzner-Jung[‡], and Anthony H. Futerman[‡3,4]

*From the [‡]Department of Biological Chemistry, Weizmann Institute of Science, Rehovot 76100, Israel, the [§]Department of Biochemistry, School of Medicine, Gachon University, Incheon 406-799, South Korea, the [¶]Department of Biochemistry, School of Medicine, Ewha Womans University, Seoul 158-710, South Korea, the [‖]Monique and Jacques Roboh Department of Genetic Research, Department of Genetics and Metabolic Diseases, Hadassah, and Hebrew University Medical Center, Jerusalem 91120, Israel, the [‡‡]Department of Pharmacology and Experimental Therapeutics, School of Pharmacy, The Hebrew University, Jerusalem 91120, Israel, and the **School of Biology and Petit Institute for Bioengineering and Bioscience, Georgia Institute of Technology, Atlanta, Georgia 30332-0230*

Background: Ceramide synthase 2 null mice cannot synthesize very long acyl chain ceramides and display severe hepatopathy.
Results: Ceramide synthase 2 null mice are protected from drug- and chemical-induced liver injury and display impaired gap junction function.
Conclusion: Altering sphingolipid levels modulates gap junction function.
Significance: Sphingolipids may play a key role in regulating drug-induced liver injury.

Very long chain (C22-C24) ceramides are synthesized by ceramide synthase 2 (CerS2). A CerS2 null mouse displays hepatopathy because of depletion of C22-C24 ceramides, elevation of C16-ceramide, and/or elevation of sphinganine. Unexpectedly, CerS2 null mice were resistant to acetaminophen-induced hepatotoxicity. Although there were a number of biochemical changes in the liver, such as increased levels of glutathione and multiple drug-resistant protein 4, these effects are unlikely to account for the lack of acetaminophen toxicity. A number of other hepatotoxic agents, such as D-galactosamine, CCl_4, and thioacetamide, were also ineffective in inducing liver damage. All of these drugs and chemicals require connexin (Cx) 32, a key gap junction protein, to induce hepatotoxicity. Cx32 was mislocalized to an intracellular location in hepatocytes from CerS2 null mice, which resulted in accelerated rates of its lysosomal degradation. This mislocalization resulted from the altered membrane properties of the CerS2 null mice, which was exemplified by the disruption of detergent-resistant membranes. The lack of acetaminophen toxicity and Cx32 mislocalization were reversed upon infection with recombinant adeno-associated virus expressing CerS2. We establish that Gap junction function is compromised upon altering the sphingolipid acyl chain length composition, which is of relevance for understanding the regulation of drug-induced liver injury.

Drug-induced liver injury (DILI)[5] is a major safety issue in the development and application of therapeutic compounds in clinical medicine (1, 2). DILI is the most frequent cause of acute liver failure in the United States, and acetaminophen (APAP) overdose is a notable cause of DILI (2). Although the underlying mechanism of DILI is not completely understood, oxidative stress caused by reactive metabolites formed during drug metabolism is believed to be involved in hepatotoxicity (3). Cytochrome p450 2E1 (CYP2E1, EC 1.14.13.n7) plays a key role in transformation of drug metabolites, and reactive metabolites can increase reactive oxygen species either through redox cycling or through GSH depletion (3).

Over the past couple of decades, vital roles for a variety of sphingolipids (SLs) in various diseases have been discovered (4, 5), suggesting that altering SL metabolism might be involved in both disease progression and, importantly, that manipulating the SL pathway might provide novel sites of therapeutic intervention.

The backbone of all SLs is (dihydro)ceramide, which is formed by the *N*-acylation of the sphingoid long chain bases sphinganine (to give dihydroceramide) or sphingosine (to give

* This work was supported, in whole or in part, by National Institutes of Health Grant GM076217. This work was also supported by the Minerva Foundation, by Israel Science Foundation Grant 0888/11, and by National Research Foundation of Korea Grants NRF-2010-357-C00069 and 2012R1A6A3A03038319 funded by the Korean Government (Ministry of Education, Science and Technology) (to J. W. P. and W. J. P.).
[S] This article contains supplemental Table 1.
[1] Both authors contributed equally to this work.
[2] Present address: Endocrinology and Metabolism Service, Dept. of Internal Medicine, Hadassah-Hebrew University Medical Center, P.O. Box 12000, Jerusalem 91120, Israel.
[3] To whom correspondence should be addressed: Dept. of Biological Chemistry, Weizmann Institute of Science, Rehovot 76100, Israel. Tel.: 972-8-9342704; Fax: 972-8-9344112; E-mail: tony.futerman@weizmann.ac.il.
[4] Joseph Meyerhoff Professor of Biochemistry at the Weizmann Institute of Science.

[5] The abbreviations used are: DILI, drug-induced liver injury; APAP, acetaminophen; SL, sphingolipid; CerS, ceramide synthase; DRM, detergent-resistant membrane; TAA, thioacetamide; Cx, connexin; MRP, multidrug resistance protein; AST, aspartate aminotransferase; ALT, alanine aminotransferase; rAAV, recombinant adeno-associated virus; WPRE, woodchuck hepatitis virus post-transcriptional element.

ceramide). The *N*-acylation reaction is governed by the ceramide synthases (CerS), of which six are known in mammals. Each CerS synthesizes ceramide with a distinct acyl chain length (6, 7). CerS2, which synthesizes C22-C24 ceramides (8), is the most ubiquitous CerS and is found at particularly high levels in the liver, kidney, and lung (8). Recently, we generated a CerS2 null mouse (9). This mouse lacks very long acyl chain (*i.e.* C22-C24) ceramides and SLs but contains elevated levels of C16-ceramide and sphinganine in the liver. CerS2 null mice display increased rates of hepatocyte death and proliferation, which results in the formation of multiple hepatic nodules and hepatocellular carcinoma (10). In addition, they have chronic oxidative stress because of disruption of the mitochondrial respiratory chain (11) and display hepatic insulin resistance because of altered detergent-resistant membranes (DRMs) (12), which appears to be related to changes in membrane biophysical properties (13, 14).

Because of these various liver pathologies, we have now examined hepatotoxicity induced by a number of drugs and chemicals. Surprisingly, CerS2 null mice were largely resistant to the hepatotoxic effects of APAP, D-galactosamine, CCl_4, and thioacetamide (TAA), mainly because of altered gap junction function as a result of mislocalization of connexin (Cx) 32, a key player in gap junctions. We suggest that the SL pathway might be a novel drug target for alleviating drug-induced liver damage and possibly other forms of acute liver failure.

EXPERIMENTAL PROCEDURES

Materials—APAP, acetaminophen sulfate, acetaminophen glucuronide, D-galactosamine, CCl_4, TAA, fumonisin B1 (FB1), MK571, chloroquine, and L-buthionine sulfoximine were from Sigma-Aldrich. Acetaminophen-glutathione (APAP-GSH) was from Santa Cruz Biotechnology. The primary antibodies used in this study were anti-Thr-183/Tyr-185-phosphorylated JNKs, anti-JNKs, anti-Ser-257/Thr-261-phosphorylated-Map kinase kinase 4 (MKK4), anti-caveolin 1, and anti-clathrin (Cell Signaling Technology); anti-nitrotyrosine (Abcam); anti-cytochrome *c* (BD Biosciences); anti-CerS2 (Sigma-Aldrich); anti-multidrug resistance protein 4 (MRP4) (EnzoLife Sciences); anti-Cx32 and anti-Cx43 (Invitrogen); and anti-GAPDH (Millipore).

Mice—CerS2 null mice were generated as described (9, 10). Mice were maintained under special pathogen-free conditions and treated in accordance with the Animal Care Guidelines of the Weizmann Institute of Science. Eight- to ten-week-old male mice were injected intraperitoneally with drugs as follows: 300 mg/kg APAP, 800 mg/kg D-galactosamine, 2 ml/kg CCl_4, and 200 mg/kg TAA. For inhibition of MRP, 25 mg/kg MK571 was injected intraperitoneally 1 h before and 1 h after APAP treatment (15). In some cases, FB1 (1.5 mg/kg/day) was injected intraperitoneally for 5 days prior to APAP treatment (16, 17). For lysosomal inhibition and GSH depletion, 50 mg/kg/day chloroquine and 3 mmol/kg/day L-buthionine sulfoximine were injected intraperitoneally for 5 days before APAP treatment (18, 19).

Serum Aspartate Aminotransferase (AST) and Alanine Aminotransferase (ALT)—Serum AST and ALT were measured by Pathovet Veterinary Diagnostic Services (Kfar Bilu, Israel) using a Roche Applied Science/Hitachi 917 system.

Histology—Liver tissues were fixed in 4% paraformaldehyde, embedded in paraffin, sectioned at 4 μm, and stained with H&E. For immunohistochemistry, paraffin sections were deparaffinized, and endogenous peroxidase activity was quenched by 0.3% (v/v) hydrogen peroxide and 0.5% (v/v) HCl in methanol. Antigen retrieval was performed using 10 mM citric acid (pH 6.0). Peroxidase activity was measured using 3,3′-diaminobenzidine as the chromogen. Sections were counterstained with hematoxylin. For immunofluorescence of tissue sections, deparaffinized liver sections were incubated with an anti-Cx32 antibody followed by a DyLight 488- or 549-conjugated secondary antibody.

Western Blotting—Livers were homogenized in radioimmune precipitation assay buffer (50 mM Tris-HCl (pH 7.5), 150 mM NaCl, 1% Nonidet P-40, 0.5% sodium deoxycholate, and 0.1% SDS) containing 50 mM NaF, 2 mM Na_3VO_4, protease inhibitors (Sigma), and phosphatase inhibitors (Sigma). Protein concentration was quantified using BCA reagent (Pierce). 50 μg of protein was separated on an 8–15% SDS-polyacrylamide gel and transferred to a nitrocellulose membrane. After blocking, membranes were incubated with primary antibodies followed by secondary antibodies (Jackson ImmunoResearch Laboratories). Chemiluminescence was performed using the SuperSignal West Pico chemiluminescent substrate (Thermo Scientific).

Electrospray Ionization-Tandem Mass Spectrometry (MS/MS)—Sphingolipid analyses by electrospray ionization-MS/MS were conducted using a PE-Sciex API 3000 triple quadrupole mass spectrometer and an ABI 4000 quadrupole linear ion trap mass spectrometer (20, 21).

GSH Analysis—Liver GSH levels were measured using a glutathione assay kit (Biovision, Mountain View, CA).

Real-time PCR—mRNA expression was determined by real-time PCR (9). Primers are listed in supplemental Table 1.

Hepatocyte Cultures—Hepatocytes were isolated from mice after hepatic portal perfusion (10). Briefly, mouse liver was perfused with Hanks' balanced salt solution (Sigma-Aldrich) containing 5.5 mM KCl, 5.5 mM glucose, 25 mM $NaHCO_3$, and 0.7 mM EDTA for 3 min and liver digest media (Invitrogen) for 8 min. After perfusion, hepatocytes were separated from connective tissue using sterile tweezers and then passed through a cell strainer (BD Falcon Labware) and centrifuged at 50 × *g* (4 °C, 5 min). Hepatocytes were suspended in DMEM containing 10% FBS, 2 mM sodium pyruvate, 2% penicillin/streptomycin, and 1 μM dexamethasone.

Tissue Scrape-and-Load Assay for Gap Junction Function—A dye solution containing 0.5% (v/v) Lucifer yellow (Invitrogen) and 0.5% (v/v) 10-kDa dextran-Texas Red (Invitrogen) was placed onto the surface of freshly prepared liver tissues, and incisions were made with a scalpel, followed by addition of an excess of dye onto the incisions (1, 22). After incubation with the dye for 5 min, liver slices were washed with phosphate-buffered saline and then fixed with 4% paraformaldehyde. Samples were frozen in optimal cutting temperature compound (Sakura Fineteck), cryosectioned at 7 μm, and mounted on slides.

Pulse-Chase—[^{35}S]methionine labeling and immunoprecipitation were performed as described (23, 24) with some modifications. Hepatocytes were starved for 1 h at 37 °C in DMEM lacking methionine and supplemented with 10% FBS and 2 mM glutamine. The medium was then replaced with fresh medium containing [^{35}S]methionine (0.1 mCi/35-mm dish). The radioactive medium was removed after 30 min, and hepatocytes were

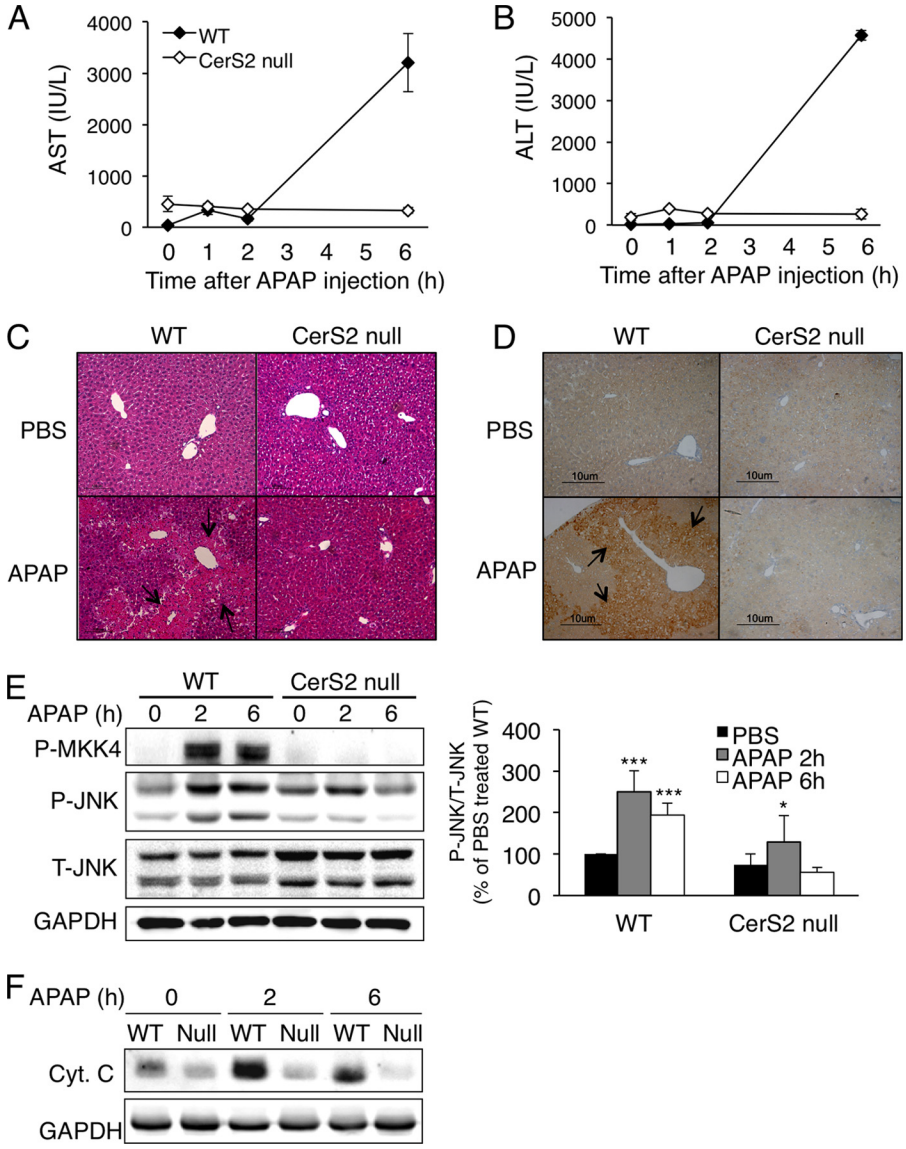

FIGURE 1. **The CerS2 null mouse is protected from APAP-induced liver injury.** AST (*A*) and ALT (*B*) were measured at the indicated times after APAP (300 mg/kg) injection. Data are mean ± S.E. $n = 3$–5. Shown are hematoxylin and eosin staining (*C*) and nitrotyrosine immunohistochemistry (*D*) after APAP (300 mg/kg) or saline injection. *Arrows* indicate damaged regions. Image magnification is ×10. *E*, representative Western blot analyses (repeated three times) of MKK4 phosphorylation at Ser-257/Thr-261 and JNK1/2 phosphorylation at Thr-183/Tyr-185 after APAP injection (*left panel*). Also shown is quantification of phosphorylated JNK/total JNK (*right panel*). Data are mean ± S.E. $n = 3$. *, $p < 0.05$; ***, $p < 0.001$. *F*, cytochrome *c* (*Cyt. C*) release into the cytosol detected by Western blotting at various times after APAP treatment. Results are representative of three independent experiments that gave similar results.

washed three times and then incubated with DMEM containing 10% FBS and 2 mM glutamine for various times (2, 4, and 8 h). At the end of the incubation period, hepatocytes were rinsed once with sterile phosphate-buffered saline at 4 °C and resuspended in lysis buffer (5 mM Tris, 5 mM EDTA, 5 mM EGTA, 10 mM iodoacetamide, 2 mM phenylmethylsulfonyl fluoride (pH 8.0), 0.6% SDS, and protease inhibitors (Sigma Aldrich)). Lysates were heated at 100 °C for 3 min to minimize aggregation of Cx32 and immunoprecipitated with an anti-Cx32 antibody and protein A-agarose (Sigma Aldrich) overnight at 4 °C. Cx32 immunoprecipitates were separated by 10% SDS-polyacrylamide gel electrophoresis, and gels were dried. The dried gels were exposed to a BioMax Transcreen LE-intensifying screen (Kodak) at −80 °C.

Detergent-Resistant Membranes (DRMs)—DRMs from liver were isolated as described (12, 25). Fresh liver tissue was homogenized in lysis buffer (0.1% Triton X-100, 100 mM NaCl, 2 mM EDTA, 2 mM EGTA, 30 mM HEPES, pH 7.5, 1 mM Na_3VO_4, 50 μM phenylarsine oxide and protease and phosphatase inhibitors). Optiprep and sucrose were added to the supernatant after centrifugation (3 min, 400 × *g*, 4 °C) to a final concentration of 40% Optiprep and 10% sucrose. Samples were overlaid with 35, 30, 25, 20, and 0% Optiprep containing 10% sucrose and centrifuged (6 h, 170,000 × *g*, 4 °C). Fractions were subsequently collected from the top of the gradient (12).

High-performance Liquid Chromatography—APAP metabolites were measured by HPLC using a C18 column (3 μm, 100 mm × 4.6 mm, Merck, Germany) (26).

Mouse Liver Mitochondria and Cytosol—Fresh liver was minced on ice and homogenized using a glass-Teflon homogenizer in 250 mM sucrose, 2 mM EDTA, 10 mM Tris (pH 7.4) and 50 IU heparin (11). Homogenates were centrifuged at 1000 × *g* for 10 min at 4 °C. The supernatant was transferred to clean

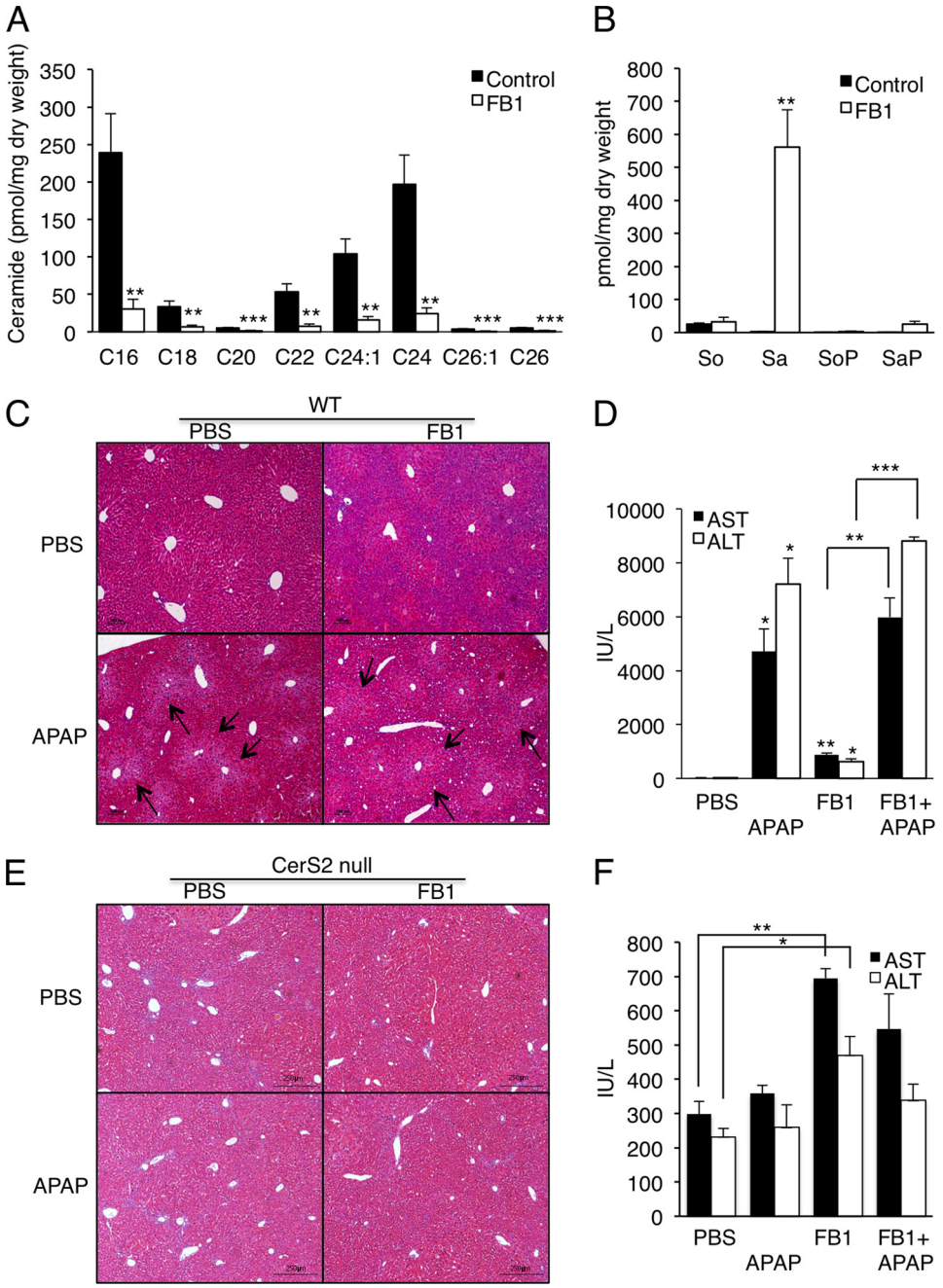

FIGURE 2. **The effect of FB1 on APAP-induced liver injury.** FB1 was injected intraperitoneally (1.5 mg/kg/day) for 5 days before treatment with APAP (300 mg/kg, 6 h). Ceramides (*A*) and long chain bases (*B*) were measured in WT liver by electrospray ionization-MS/MS. The *x* axis in *A* shows the acyl chain lengths of the individual ceramide species. *So*, sphingosine; *Sa*, sphinganine; *SoP*, sphingosine 1 phosphate; *SaP*, sphinganine 1 phosphate. Data are mean ± S.E. $n = 3–4$. **, $p < 0.01$; ***, $p < 0.001$. *C*, hematoxylin and eosin staining of WT liver after 5 days of FB1 treatment (1.5 mg/kg/day) and/or APAP (300 mg/kg, 6 h). This experiment was repeated three times with similar results. *Arrows* indicate damaged regions. Image magnification is ×10. *D*, serum AST and ALT levels. Data are mean ± S.E. $n = 3–4$. *, $p < 0.05$; **, $p < 0.01$; ***, $p < 0.001$. *E*, hematoxylin and eosin staining of CerS2 null mouse liver after 5 days of FB1 treatment (1.5 mg/kg/day) and/or APAP (300 mg/kg, 6 h). This experiment was repeated three times with similar results. Image magnification is ×10. *F*, serum AST and ALT levels. Data are mean ± S.E. $n = 3$. *, $p < 0.05$; **, $p < 0.01$.

tubes and centrifuged again at 14,000 × *g* for 15 min at 4 °C. The supernatant was used as the cytosolic fraction to detect cytochrome *c* release.

Recombinant Adeno-associated Virus—The pAAV2-EF-hCERS2-WPRE vector containing full-length human CerS2 cDNA under the human elongation factor (EF) 1-α promoter and downstream woodchuck hepatitis virus posttranscriptional element (WPRE) as well as bovine growth hormone poly (A) signal were created by replacing the eGFP cDNA in the pAAV-EF-eGFP-WPRE-BGH poly(A) vector with human CerS2 cDNA (27). The rep2/cap8 plasmid (p5E18-VD2/8, provided by Dr. Sung-Chul Jung (28, 29), was used to package the expression vector. The recombinant adeno-associated virus (rAAV) carrying human CerS2 (rAAV2/8-CerS2) or GFP (rAAV2/8-eGFP) vectors were produced by the triple plasmid transfection method and purified by cesium chloride density gradient ultracentrifugation (28, 30). The rAAV genomic titer was calculated using real-time PCR in which the signal from aliquots of the test

material were compared with a standard signal generated using the linearized pAAV2-EF-hCerS2-WPRE plasmid or pAAV-EF-eGFP-WPRE plasmid (28).

Statistics—Values are given as means ± S.E. Unless stated otherwise, statistical significance was calculated using Student's *t* test, and $p < 0.05$ was considered statistically significant.

RESULTS

Lack of APAP Hepatotoxicity in CerS2 Null Mice—CerS2 null mice were completely protected from the hepatotoxic effects of APAP (Fig. 1). Although WT mice displayed huge elevations in serum AST (Fig. 1*A*) and ALT (*B*) levels 6 h after APAP injection, no changes were detected in CerS2 null mice, indicating a lack of APAP-induced liver damage, which was confirmed by morphological analyses (H&E staining, *C*) and analysis of formation of nitrotyrosine protein adducts (*D*), which demonstrated significant damage in WT mouse liver but not in CerS2 null mouse liver. We also examined a number of signaling pathways involved in APAP-induced liver injury. Consistent with lower levels of reactive oxygen species generated from mitochondria by treatment with APAP (3454 ± 476 in WT *versus* 1453 ± 243 of relative fluorescence unit in CerS2 null mice), MKK4 (31) was not activated upon APAP injection in CerS2 null mice (Fig. 1*E*). Likewise, JNKs were only transiently activated (Fig. 1*E*), and, consequently, cytochrome *c* was not released into the cytosol in CerS2 null mouse liver (*F*), indicating that mitochondria were not damaged by APAP treatment.

In addition to the reduction in very long chain (C22-C24) and elevation in C16-ceramide levels, CerS2 null mouse liver displays a significant elevation in sphinganine levels (9). To determine whether elevated sphinganine might be responsible for the lack of hepatotoxicity, WT mice were injected with the CerS inhibitor FB1 (16, 17) for 5 days prior to APAP injection. As

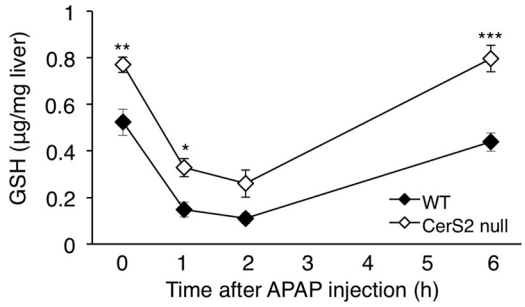

FIGURE 3. **Increased GSH in CerS2 null mouse liver.** *A*, GSH levels were measured in CerS2 null and WT liver at the indicated times after APAP (300 mg/kg) injection. Data are mean ± S.E. $n = 3–6$. *, $p < 0.05$; **, $p < 0.01$; ***, $p < 0.001$.

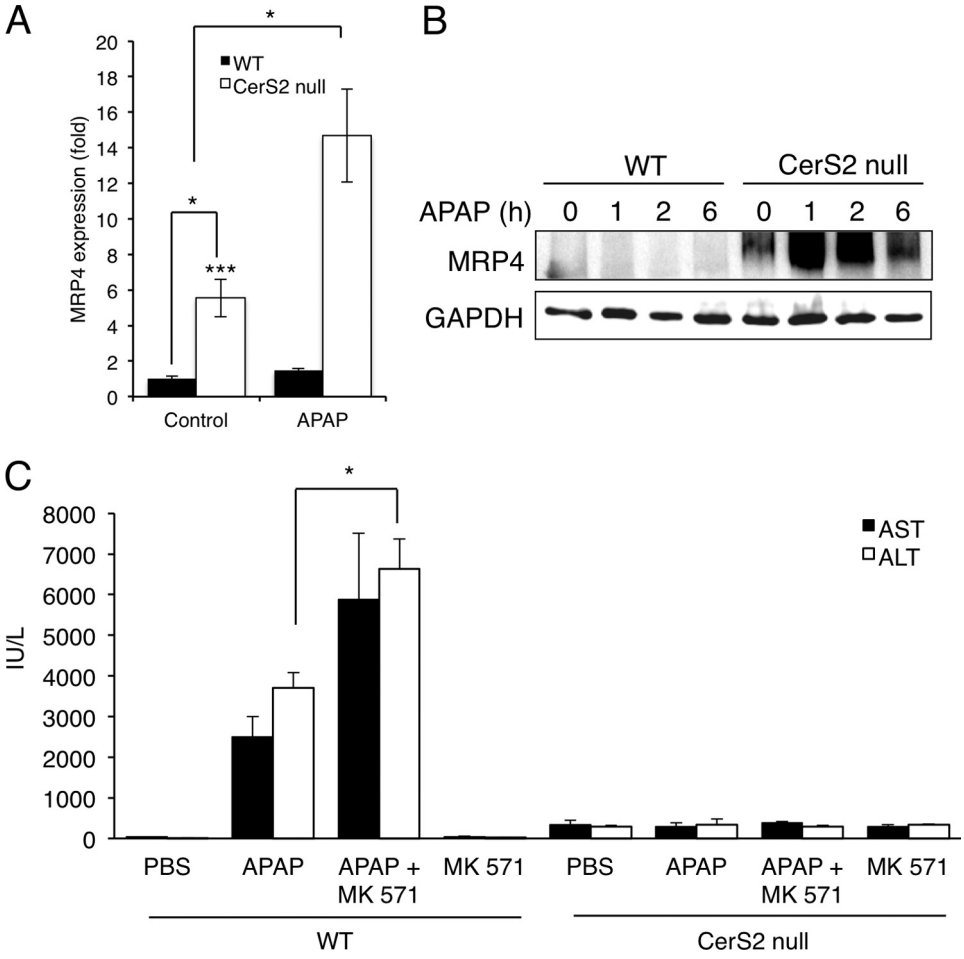

FIGURE 4. **Elevated MRP4 in CerS2 null mouse liver.** *A*, real-time PCR of MRP4 before and after APAP (300 mg/kg, 6 h) injection. Data are mean ± S.E. $n = 3$. *, $p < 0.05$; ***, $p < 0.001$. *B*, representative Western blot analyses (repeated three times) of MRP4 levels after APAP (300 mg/kg) injection. *C*, the MRP inhibitor MK571 (25 mg/kg) was injected intraperitoneally 1 h before and 1 h after APAP treatment. Serum AST and ALT were analyzed 6 h after APAP injection. Data are mean ± S.E. $n = 3–6$. *, $p < 0.05$.

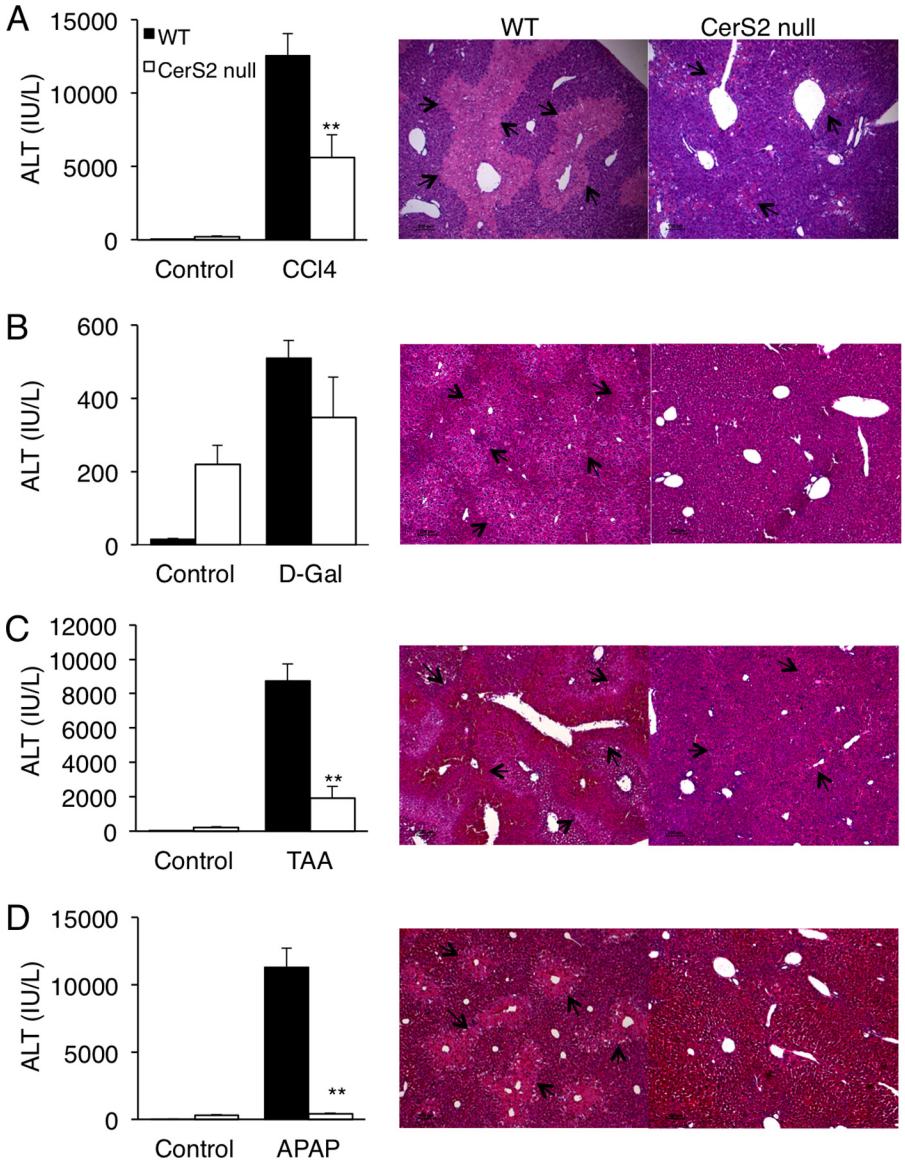

FIGURE 5. **The CerS2 null mouse is protected from chemically induced liver injury.** Serum ALT levels and hematoxylin and eosin staining 24 h after CCl_4 (2 ml/kg) (*A*), D-Galactosamine (*D-Gal*, 800 mg/kg) (*B*), TAA (200 mg/kg) (*C*), and APAP (300 mg/kg) (*D*) administration. Data are mean ± S.E. $n = 3–4$. Hematoxylin and eosin staining is representative of three independent experiments. *Arrows* indicate damaged regions. Image magnification is ×10. Data are mean ± S.E. $n = 3–4$. **, $p < 0.01$.

expected, FB1 injection reduced ceramide and elevated sphinganine levels and caused some liver damage similar to that reported previously (16, 17) (Fig. 2, *A* and *B*). However, FB1 administration did not alleviate APAP-induced centrilobular liver damage or APAP-induced elevation of liver enzymes in the serum of WT mice (Fig. 2, *C* and *D*). Likewise, FB1 administration to CerS2 null mice did not affect APAP toxicity (Fig. 2, *E* and *F*). Therefore, we conclude that elevated sphinganine and increased C16-ceramides are not likely to be directly involved in the protective mechanism of APAP-induced hepatotoxicity.

Elevated GSH May Be Partially Responsible for Lack of APAP Hepatotoxicity—We first examined APAP metabolism. APAP is metabolized to the active metabolite *N*-acetyl-*p*-benzoquinone imine by Cyp2E1. However, Cyp2E1 activity and expression were unaltered in CerS2 null mice both before (821.67 ± 13 pmol/min/mg) and after (692 ± 97.2 pmol/min/mg) APAP injection. We next examined levels of GSH because GSH depletion is one of the main mechanisms of APAP-induced liver damage (3, 32). GSH levels were elevated 1.5-fold in CerS2 null liver prior to APAP injection and decreased to a similar extent as in WT mice after APAP injection (Fig. 3). However, levels of unmetabolized APAP were lower in liver (3146.7 ± 461.6 in WT *versus* 1100.7 ± 302.3 nmol/g in CerS2 null mice) and in plasma (873.1 ± 112.3 *versus* 428.7 ± 63.9 nmol/ml) with a concomitant increase in APAP-GSH in liver (1567.6 ± 170.7 *versus* 3172.7 ± 578.8 nmol/g), demonstrating that APAP detoxification by GSH is increased in CerS2 null liver. We conclude that changes in APAP metabolism may be partly responsible for the lack of APAP toxicity in CerS2 null mice, although it is unlikely to be the major mechanism because CerS2 null mice were also resistant to other hepatotoxins (see below).

Multidrug-resistant pumps are responsible for the removal of toxic drugs from the liver (33), and, specifically, MRP4 may

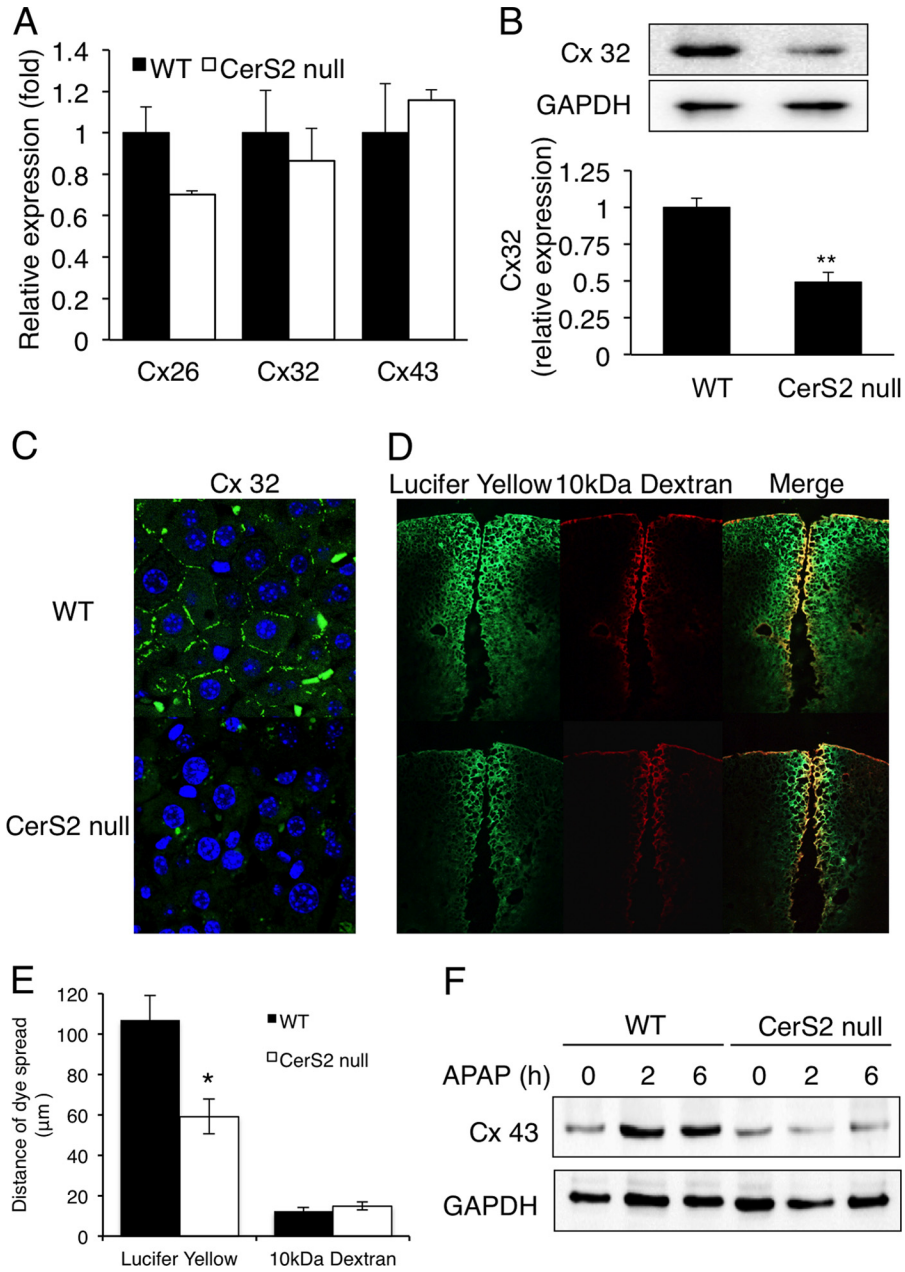

FIGURE 6. **Hepatic gap junction dysfunction in CerS2 null liver.** *A*, real-time PCR of hepatic Cx genes. Data are mean ± S.E. $n = 4$. *B*, representative Western blot analyses (*top panel*) and quantification (*bottom panel*) ($n = 4$) of Cx32 levels. Data are mean ± S.E. **, $p < 0.01$. *C*, immunofluorescence staining of Cx32 in liver. Image magnification is ×100. *D*, tissue scrape-and-load assay for gap junction function using Lucifer yellow (which is gap junction-permeable) and 10 kDa dextran-Texas Red (which is gap junction-impermeable). Image magnification is ×10. *E*, quantification of the distance of dye spread of Lucifer yellow and 10 kDa dextran. Data are mean ± S.E. $n = 4$. *, $p < 0.05$. *F*, Western blot analysis of Cx43 levels at various times after APAP treatment (300 mg/kg, intraperitoneally). This experiment was repeated three times with similar results.

protect against APAP-induced liver injury (34–36). Because plasma acetaminophen-glucuronide levels (472.2 ± 39.7 in WT *versus* 687.9 ± 48.5 nmol/ml in CerS2 null mice) and acetaminophen sulfate (77.6 ± 6.6 in WT *versus* 109.2 ± 5.4 nmol/ml in CerS2 null mice) were elevated somewhat in CerS2 null mice, we examined whether multidrug-resistant pumps are altered in CerS2 null mouse liver. Levels of MRP4 mRNA and MRP4 protein were significantly elevated in CerS2 null mouse liver (Fig. 4, *A* and *B*). However, treatment with the MRP inhibitor MK571 (15) had no effect on APAP-induced hepatotoxicity in CerS2 null mice, whereas it induced ALT elevation in WT mice (Fig. 4*C*), suggesting that elevated levels of MRP4 are not responsible for the lack of APAP-mediated hepatotoxicity in CerS2 null mice. In summary, although the above mechanisms might contribute, at least partially, to the lack of APAP hepatotoxicity in CerS2 null mice, it seems likely that additional mechanisms are involved.

Impaired Gap Junction Function in CerS2 Null Mouse Liver—We next treated CerS2 null mice with a variety of other hepatotoxic agents that each cause liver damage by a different mechanism (37, 38). Remarkably, three other chemicals, namely CCl_4, D-galactosamine, and TAA were also ineffective in inducing hepatotoxicity, although the extent of protection differed for each (Fig. 5).

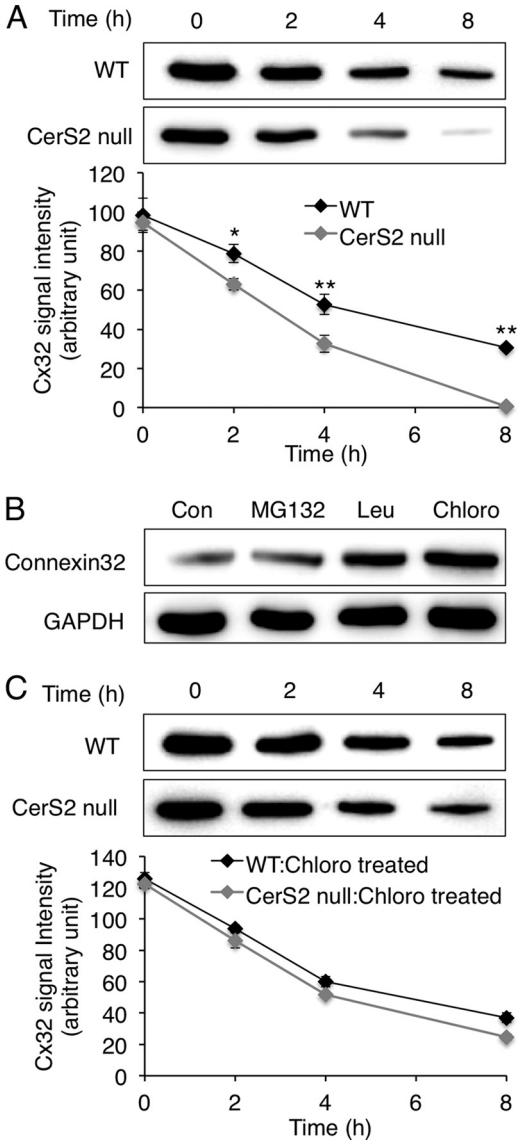

FIGURE 7. **Reversal of Cx32 degradation by inhibition of lysosomal proteases.** *A*, pulse-chase experiment using [^{35}S]methionine (top *panel*) and quantification (*bottom panel*) in hepatocytes from WT and CerS2 null mice. This experiment was repeated three times with similar results. Data are mean ± S.E. $n = 3$. *, $p < 0.05$; **, $p < 0.01$. *B*, hepatocytes were incubated with MG132 (20 μM), leupeptin (*Leu*, 100 μM), or chloroquine (*Chloro*, 100 μM) for 6 h, and Cx32 levels were measured by Western blotting. GAPDH is shown as a loading control (*Con*). *C*, pulse-chase experiment using [^{35}S]methionine (*top panel*) and quantification (*bottom panel*) in WT and chloroquine-treated (100 μM) CerS2 null mouse hepatocytes. This experiment was repeated three times with similar results.

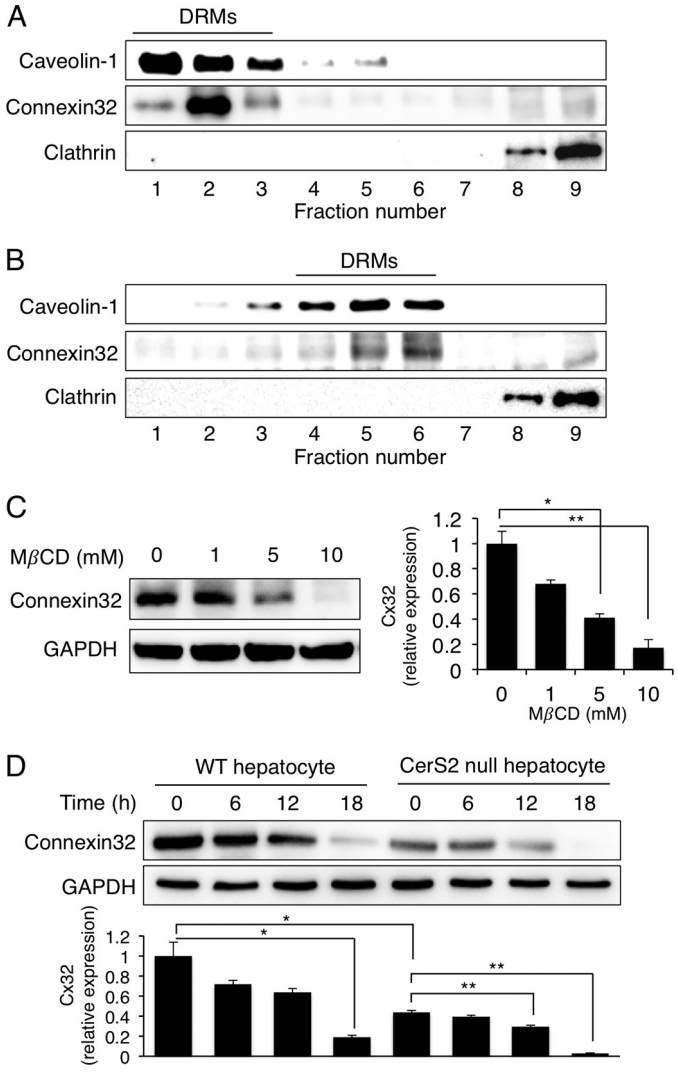

FIGURE 8. **Cx32 levels are reduced by disruption of DRMs.** *A* and *B*, localization of Cx32 in Optiprep density fractions of WT (*A*) and CerS2 null (*B*) mice. Caveolin 1 and clathrin were used as markers of DRM and non-DRM fractions, respectively. Results are representative of three independent experiments. *C*, effect of different amounts of methyl-β-cyclodextrin (*MβCD*) (12 h) on Cx32 levels in WT hepatocytes (*left panel*) and quantification (*right panel*). Data are mean ± S.E. $n = 3$. *, $p < 0.05$; **, $p < 0.01$. *D*, effect of different times of treatment with MβCD (5 mM) on Cx32 levels (*top panel*) and quantification (*bottom panel*). Data are mean ± S.E. $n = 3$. *, $p < 0.05$; **, $p < 0.01$.

Gap junctions have recently been implicated in the hepatotoxicity of all four of the drugs and chemicals used in this study by the demonstration that ablation of Cx32 (a key protein in hepatic gap junctions) completely protects against DILI (1, 39, 40). Thus, we examined Cx levels and gap junction function in CerS2 null liver. mRNA levels of Cx26, 32, and 43 were not altered (Fig. 6*A*), but levels of the Cx32 protein were decreased significantly in CerS2 null mouse liver as detected by Western blotting (*B*) and immunofluorescence (*C*). Gap junction function, assayed using a tissue scrape-load assay, was also compromised severely (Fig. 6, *D* and *E*). Similar to results obtained in a Cx32-deficient rat (41), Cx43 expression did not increase in CerS2 null mouse liver after APAP injection, in contrast to a significant elevation in WT mice (which indicates hepatocyte damage (3, 41)) (Fig. 6*F*).

Because Cx32 mRNA levels were unaltered in CerS2 null mouse liver (Fig. 6*A*), we analyzed the rate of degradation of Cx32 by pulse-chase using [^{35}S]methionine. Cx32 degradation was significantly faster in hepatocytes obtained from CerS2 null mice (half-life, 4.4 ± 0.2 h in WT *versus* 2.4 ± 0.4 h in CerS2 null mice) (Fig. 7*A*). Interestingly, Cx32 could be restored to levels similar to those found in the WT upon incubation with the lysosomal protease inhibitors leupeptin or chloroquine (19) but not upon incubation with the proteasomal inhibitor MG132 (Fig. 7*B*). Lysosomal inhibition in CerS2 null hepatocytes also slowed down the rate of Cx32 degradation so that it was similar to the rate of degradation in the WT (half-life of 4.6 ± 0.5 h in WT *versus* 4.2 ± 0.2 h in CerS2 null mice) (Fig. 7*C*).

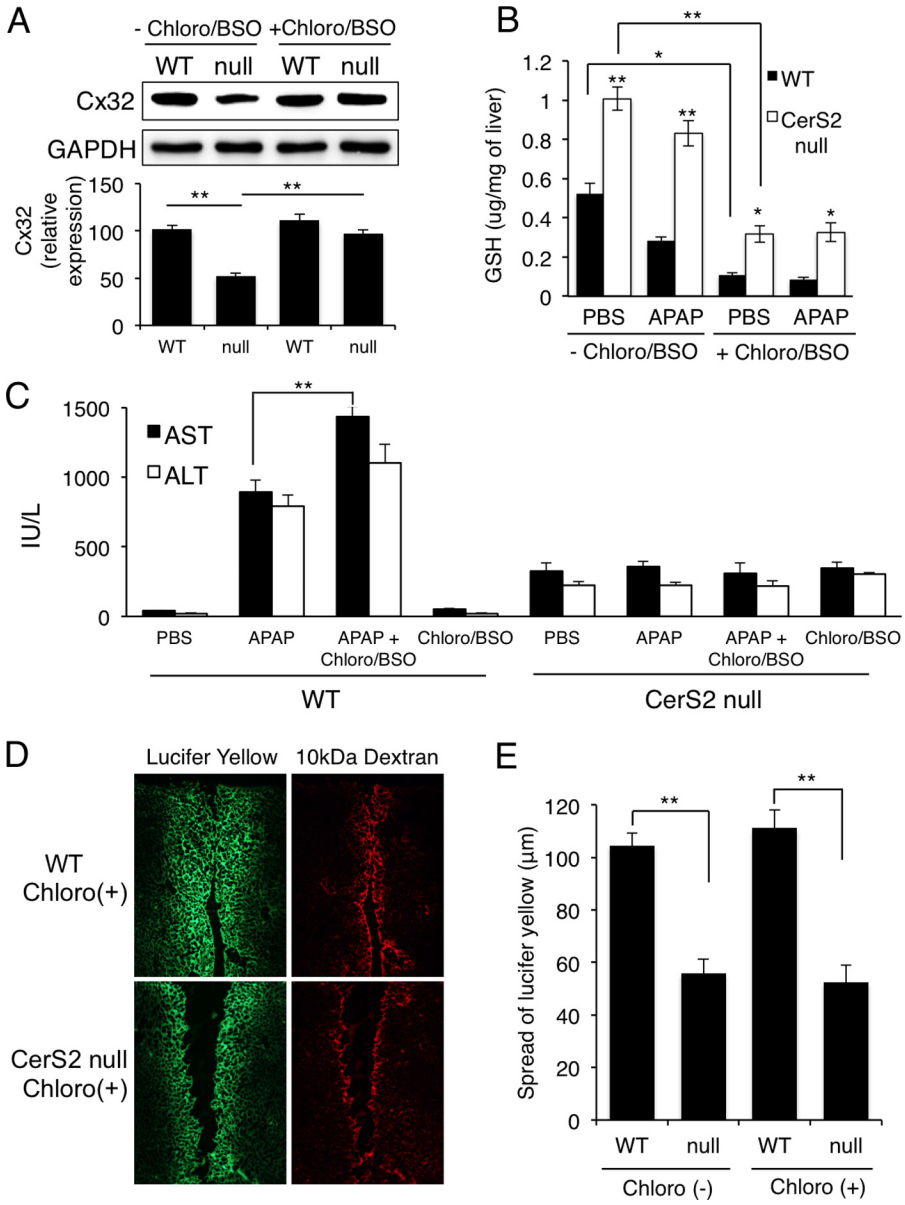

FIGURE 9. **Recovery of Cx32 levels in CerS2 null mice did not reverse the protection against APAP-induced liver damage.** Chloroquine (*Chloro*, 50 mg/kg/day) and L-buthionine sulfoximine (BSO) (3 mmol/kg/day) were injected intraperitoneally for 5 days before APAP injection. *A*, representative Western blot analyses (*top panel*) and quantification (*bottom panel*) of Cx32 levels. Data are mean ± S.E. $n = 3$. **, $p < 0.01$. *B*, GSH was measured 6 h after APAP (300 mg/kg) injection. Values are mean ± S.E. $n = 3$. *, $p < 0.05$; **, $p < 0.01$. *C*, serum AST and ALT levels. Data are mean ± S.E. $n = 3$. **, $p < 0.01$. *D*, tissue scrape-and-load assay. This experiment was repeated three times with similar results. Image magnification is ×10. *E*, distance of spread of Lucifer yellow dye. Data are mean ± S.E. $n = 3$. **, $p < 0.01$.

Cx32 localizes to DRMs (42). We demonstrated recently that the density and composition of DRMs differ in CerS2 null mice (12), along with changes in the biophysical properties of membranes (13, 14). Although Cx32 localized to DRMs isolated from the liver of both WT (Fig. 8*A*) and CerS2 null mice (*B*), the density of the DRMs differed between the two, and the extent of co-localization was significantly lower in CerS2 null mice (*B*). Disruption of DRMs isolated from hepatocytes using methyl-β-cyclodextrin decreased Cx32 levels in a dose- (Fig. 8*C*) and time-dependent (*D*) manner, consistent with the idea that Cx32 degradation is accelerated upon disruption of DRMs, as occurs upon changing the SL acyl chain composition in the CerS2 null mouse.

To determine the role of enhanced Cx32 degradation in the protection against APAP-induced liver injury, mice were injected with chloroquine together with BSO (an inhibitor of GSH synthesis) for 5 days prior to APAP injection. As expected, CX32 levels increased in the CerS2 null mouse to a similar level to that of the WT (Fig. 9*A*), and there was a significant decrease in GSH levels (*B*). However, CerS2 null mice were still protected from APAP-induced liver injury upon pretreatment with chloroquine and BSO, as demonstrated by the lack of change in liver function (AST and ALT levels, Fig. 9*C*) and gap junction function (tissue scrape-load assay, *D* and *E*). Rather, the intracellular transport of Cx32 is defective in CerS2 null mouse hepatocytes irrespective of its intracellular levels. Thus, although Cx32 is localized to the plasma membrane in hepatocytes from WT mice, it is localized intracellularly in hepatocytes from CerS2 null mice irrespective of whether its levels are increased by inhi-

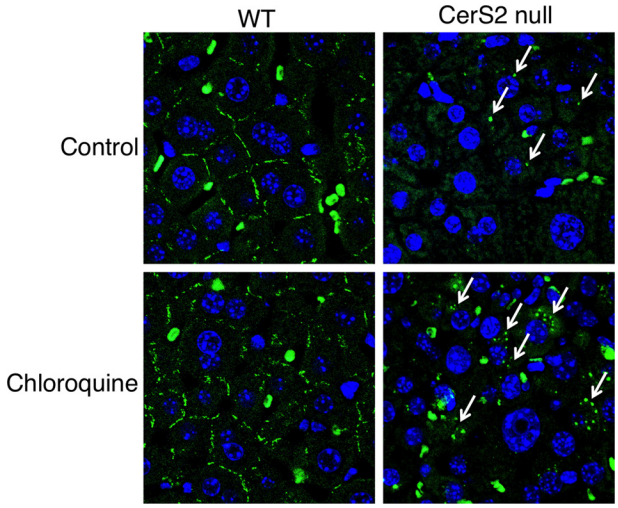

FIGURE 10. **Mislocalization of Cx32 in CerS2 null liver.** WT and CerS2 null mice were treated with chloroquine (50 mg/kg/day for 5 days), and Cx32 localization was determined by immunofluorescence. *Arrows* indicate the intracellular site of Cx32 accumulation in CerS2 null liver. Image magnification is ×100.

bition of lysosomal degradation (Fig. 10). The inability of Cx32 to be transported to the plasma membrane provides a mechanistic explanation of the protection of CerS2 null mice against DILI.

To attempt to reverse the lack of APAP hepatotoxicity in CerS2 null mice, we generated rAAV expressing CerS2. CerS2 null mice were infected via tail vein injection of 2×10^{12} viral particles. After 5 weeks, CerS2 protein levels were increased significantly with a concomitant elevation of Cx32 levels (Fig. 11*A*). When 300 mg/kg APAP was injected into CerS2 null mice that had been infected with rAAV-CerS2, serum AST and ALT levels were elevated, demonstrating significant hepatotoxicity (Fig. 11*B*), which was confirmed by H&E staining (*C*). Finally, although Cx32 levels were localized intracellularly in CerS2 null mice, rAAV-CerS2 infection resulted in its retargeting to the plasma membrane (Fig. 11*D*). Together, the rAAV-CerS2 infection experiments demonstrate a direct mechanistic link between levels of CerS2 and APAP-induced hepatotoxicity.

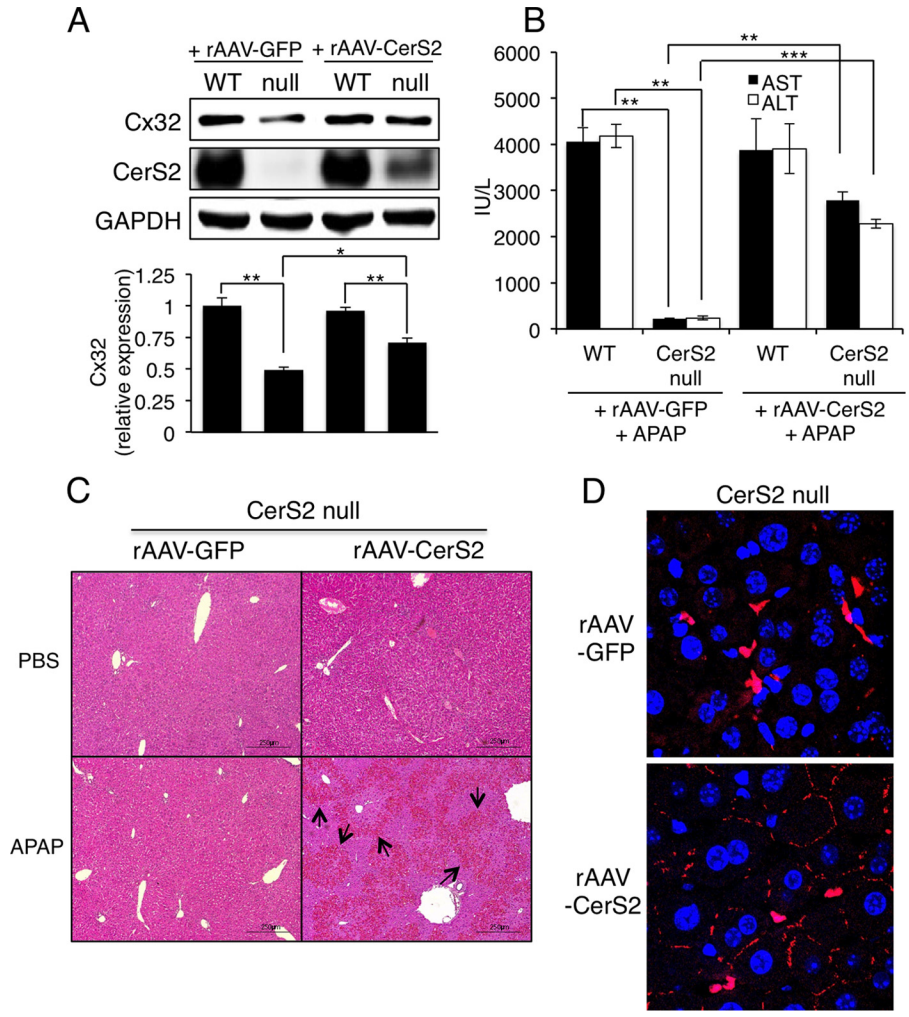

FIGURE 11. **rAAV-CerS2 infection reverses the lack of APAP hepatotoxicity in CerS2 null mice.** Recombinant rAAV-CerS2 or rAAV-GFP (2×10^{12} viral particles) were injected into WT or CerS2 null mice 5 weeks prior to APAP (300 mg/kg) treatment. *A*, representative Western blot analyses (*top panel*) of CerS2 and Cx32 levels and quantification (*bottom panel*) ($n = 3$) of Cx32 levels. Data are mean ± S.E. *, $p < 0.05$; **, $p < 0.01$. *B*, serum AST and ALT levels after APAP treatment. Data are mean ± S.E. **, $p < 0.01$; ***, $p < 0.001$. *C*, hematoxylin and eosin staining after PBS or APAP treatment. *D*, immunofluorescence staining of Cx32 in liver after injection of rAAV-CerS2 or rAAV-GFP. Image magnification is ×100.

DISCUSSION

In this study we demonstrate that, despite the severe hepatopathy observed in CerS2 null mice, these mice are resistant to drug- and chemical-induced liver injury. The molecular mechanisms underlying this resistance may involve a combination of factors, but the most likely mechanism is the mislocalization and, hence, an enhanced rate of degradation, of a major player in gap junction function, namely Cx32. This is strongly supported by the ability to reverse the mislocalization of Cx32 using rAAV-CerS2.

Gap junctions have recently emerged as important players in regulating DILI (1, 39). Gap junction channels consist of Cx proteins and are involved in intercellular communication and in the amplification of liver inflammation and injury (1, 39, 41, 43). Ablation of Cx32, a major Cx in liver, abrogates liver injury induced by the same four hepatotoxic agents used in this study (1, 39–41), and APAP-induced-Cx43 expression was inhibited in Cx32 dominant-negative transgenic rats (41) similar to that observed in the CerS2 null mouse.

Our data are consistent with the following model. Changes in the acyl chain length of sphingolipids leads to altered biophysical properties of membranes (14) that are exemplified by changes in the properties of DRMs. Although the use of DRMs as a measure of membrane properties is clouded in controversy (44), they do nevertheless provide a quick and simple way to measure some changes in membrane characteristics. We previously demonstrated altered DRMs in the CerS2 null mouse, which results in defective insulin receptor signaling (12) and in the internalization of the TNFα receptor.[6] We now suggest that the altered biophysical properties of hepatocyte membranes results in the mislocalization of Cx32. Whether the mislocalization is due to defective assembly, transport along the secretory pathway, or defective internalization remains to be established. In CerS2 null mice, the rate of Cx32 degradation is increased, perhaps because of its instability in the altered membrane environment of CerS2 null mouse hepatocytes. The increased rate of Cx32 degradation is directly related to lysosomal proteolytic degradation, but even inhibition of lysosomal degradation does not result in the correct localization of Cx32 to the plasma membrane, even though it does restore its intracellular levels. Finally, reintroduction of CerS2 into CerS2 null liver using rAAV-CerS2 corrected the Cx32 mislocalization, supporting the idea that altered membrane properties caused by lack of CerS2 are a major reason for Cx32 mislocalization. Thus, we suggest that the increased rate of lysosomal degradation is the result of the instability of Cx32 rather than the cause of reduced Cx32 levels. Previous studies have shown that misfolded connexins are more vulnerable to proteasomal degradation (23), and we now suggest that Cx32 is also more vulnerable to lysosomal degradation.

A number of other pathways are altered in the CerS2 null mouse. CerS2 null mice display chronic oxidative stress caused by high sphinganine and C16-ceramide (11), which may also contribute to the augmented Cx32 degradation (45). In addition, altered drug metabolism, higher GSH levels, and other downstream signaling pathways may all play a part in the lack of APAP-induced liver damage, but we surmise that these pathways are likely to play minor roles because of the lack of commonality of these pathways in the effects of the four hepatotoxic agents used in this study. For example, CYP2E1 is required to transform many drugs but is not involved in D-galactosamine metabolism. Apoptosis signal-regulating kinase 1 knockout mice are protected from APAP- and TNFα-induced hepatotoxicity but not from CCl_4- or Fas-induced liver injury (38), and treatment with a JNK inhibitor alleviates APAP- and TNFα-induced liver injury but does not affect CCl_4- or Fas-induced liver injury (46). In contrast, oxidative stress, mitochondrial dysfunction, and GSH depletion are all commonly involved in DILI (3) and are all altered in the CerS2 null mouse. However, as discussed above, these factors are likely to play a minor role in the protection against DILI in the CerS2 null mouse.

Although the CerS2 null mouse was protected from chemically induced liver injury, the extent of protection differed depending on the drug. For example, the CerS2 null mouse was only partially protected from CCl_4-induced hepatotoxicity in contrast to complete protection from APAP-induced liver injury. Along with impaired gap junction function, mRNA levels of dual specificity phosphatases (including dual specificity phosphatases 8 and 10) were elevated (27.1 $\pm$ 5.4- and 7.5 $\pm$ 1.1-fold, respectively). Because a JNK inhibitor alleviates APAP-induced hepatotoxicity but not CCl_4-induced hepatotoxicity (46), the different extent of protection against DILI in the CerS2 null mouse could be explained by an elevation of dual specificity phosphatases because of their role as JNK phosphatases (47).

SLs are now known to be important mediators in many cellular processes. This study suggests that SLs are also involved in regulating the function of proteins and pathways involved in DILI, perhaps because these proteins need a specific membrane environment to function properly. This is exemplified by the altered localization of Cx32 in CerS2 null mice. It is to be expected that other membrane proteins, involved in a number of other physiological and pathophysiological pathways, will be modulated upon alteration of the acyl chain composition of membrane SLs.

Acknowledgments—We thank Drs. Oren Tirosh (Hebrew University of Jerusalem) and Ori Brenner (Weizmann Institute of Science) for helpful comments; Dr. Elad L. Laviad (Weizmann Institute of Science), Dr. Meidan Goldfinger (Hebrew University of Jerusalem), Seung-Hoon Yang (Weizmann Institute of Science), and Dr. Sung-Chul Jung (Ewha Womans University) for technical assistance; and Dr. Arthur Cerderbaum (Mount Sinai School of Medicine) for measurement of Cyp2E1 activity.

[6] M. Ali, J. Fritsch, H. Zigdon, Y. Pewzner Jung, S. Schütze, and A. H. Futerman, submitted for publication.

REFERENCES

1. Patel, S. J., Milwid, J. M., King, K. R., Bohr, S., Iracheta-Velle, A., Li, M., Vitalo, A., Parekkadan, B., Jindal, R., and Yarmush, M. L. (2012) Gap junction inhibition prevents drug-induced liver toxicity and fulminant hepatic failure. *Nat. Biotechnol.* **30,** 179–183
2. Holt, M. P., and Ju, C. (2006) Mechanisms of drug-induced liver injury. *AAPS J.* **8,** E48–E54

3. Han, D., Shinohara, M., Ybanez, M. D., Saberi, B., and Kaplowitz, N. (2010) Signal transduction pathways involved in drug-induced liver injury. *Handb. Exp. Pharmacol.* **196,** 267–310
4. van Echten-Deckert, G., and Walter, J. (2012) Sphingolipids. Critical players in Alzheimer's disease. *Prog. Lipid Res.* **51,** 378–393
5. Chavez, J. A., and Summers, S. A. (2012) A ceramide-centric view of insulin resistance. *Cell Metab.* **15,** 585–594
6. Pewzner-Jung, Y., Ben-Dor, S., and Futerman, A. H. (2006) When do Lasses (longevity assurance genes) become CerS (ceramide synthases)? Insights into the regulation of ceramide synthesis. *J. Biol. Chem.* **281,** 25001–25005
7. Mullen, T. D., Hannun, Y. A., and Obeid, L. M. (2012) Ceramide synthases at the centre of sphingolipid metabolism and biology. *Biochem. J.* **441,** 789–802
8. Levy, M., and Futerman, A. H. (2010) Mammalian ceramide synthases. *IUBMB Life* **62,** 347–356
9. Pewzner-Jung, Y., Park, H., Laviad, E. L., Silva, L. C., Lahiri, S., Stiban, J., Erez-Roman, R., Brügger, B., Sachsenheimer, T., Wieland, F., Prieto, M., Merrill, A. H., Jr., and Futerman, A. H. (2010) A critical role for ceramide synthase 2 in liver homeostasis. I. Alterations in lipid metabolic pathways. *J. Biol. Chem.* **285,** 10902–10910
10. Pewzner-Jung, Y., Brenner, O., Braun, S., Laviad, E. L., Ben-Dor, S., Feldmesser, E., Horn-Saban, S., Amann-Zalcenstein, D., Raanan, C., Berkutzki, T., Erez-Roman, R., Ben-David, O., Levy, M., Holzman, D., Park, H., Nyska, A., Merrill, A. H., Jr., and Futerman, A. H. (2010) A critical role for ceramide synthase 2 in liver homeostasis. II. Insights into molecular changes leading to hepatopathy. *J. Biol. Chem.* **285,** 10911–10923
11. Zigdon, H., Kogot-Levin, A., Park, J.-W., Goldschmidt, R., Kelly, S., Merrill, A. H., Jr., Scherz, A., Pewzner-Jung, Y., Saada, A., and Futerman, A. H. (2013) Ablation of ceramide synthase 2 causes chronic oxidative stress due to disruption of the mitochondrial respiratory chain. *J. Biol. Chem.* **288,** 4947–4956
12. Park, J.-W., Park, W.-J., Kuperman, Y., Boura-Halfon, S., Pewzner-Jung, Y., and Futerman, A. H. (2013) Ablation of very long acyl chain sphingolipids causes hepatic insulin resistance in mice due to altered detergent-resistant membranes. *Hepatology* **57,** 525–532
13. Yurlova, L., Kahya, N., Aggarwal, S., Kaiser, H.-J., Chiantia, S., Bakhti, M., Pewzner-Jung, Y., Ben-David, O., Futerman, A. H., Brügger, B., and Simons, M. (2011) Self-segregation of myelin membrane lipids in model membranes. *Biophys. J.* **101,** 2713–2720
14. Silva, L. C., Ben David, O., Pewzner-Jung, Y., Laviad, E. L., Stiban, J., Bandyopadhyay, S., Merrill, A. H., Jr., Prieto, M., and Futerman, A. H. (2012) Ablation of ceramide synthase 2 strongly affects biophysical properties of membranes. *J. Lipid Res.* **53,** 430–436
15. Hara, Y., Sassi, Y., Guibert, C., Gambaryan, N., Dorfmüller, P., Eddahibi, S., Lompré, A.-M., Humbert, M., and Hulot, J.-S. (2011) Inhibition of MRP4 prevents and reverses pulmonary hypertension in mice. *J. Clin. Invest.* **121,** 2888–2897
16. Dugyala, R. R., Sharma, R. P., Tsunoda, M., and Riley, R. T. (1998) Tumor necrosis factor-α as a contributor in fumonisin B1 toxicity. *J. Pharmacol. Exp. Ther.* **285,** 317–324
17. Tsunoda, M., Sharma, R. P., and Riley, R. T. (1998) Early fumonisin B1 toxicity in relation to disrupted sphingolipid metabolism in male BALB/c mice. *J. Biochem. Mol. Toxicol.* **12,** 281–289
18. Andersen, J. K., Mo, J. Q., Hom, D. G., Lee, F. Y., Harnish, P., Hamill, R. W., and McNeill, T. H. (1996) Effect of buthionine sulfoximine, a synthesis inhibitor of the antioxidant glutathione, on the murine nigrostriatal neurons. *J. Neurochem.* **67,** 2164–2171
19. Berthoud, V. M., Tadros, P. N., and Beyer, E. C. (2000) Connexin and gap junction degradation. *Methods* **20,** 180–187
20. Sullards, M. C., Liu, Y., Chen, Y., and Merrill, A. H. (2011) Analysis of mammalian sphingolipids by liquid chromatography tandem mass spectrometry (LC-MS/MS) and tissue imaging mass spectrometry (TIMS). *Biochim. Biophys. Acta* **1811,** 838–853
21. Shaner, R. L., Allegood, J. C., Park, H., Wang, E., Kelly, S., Haynes, C. A., Sullards, M. C., and Merrill, A. H. (2009) Quantitative analysis of sphingolipids for lipidomics using triple quadrupole and quadrupole linear ion trap mass spectrometers. *J. Lipid Res.* **50,** 1692–1707
22. Upham, B. L. (2011) Role of integrative signaling through gap junctions in toxicology. *Curr. Protoc. Toxicol.* Chapter 2, Unit 2.18
23. Musil, L. S., Le, A. C., VanSlyke, J. K., and Roberts, L. M. (2000) Regulation of connexin degradation as a mechanism to increase gap junction assembly and function. *J. Biol. Chem.* **275,** 25207–25215
24. Le, A. C., and Musil, L. S. (1998) Normal differentiation of cultured lens cells after inhibition of gap junction-mediated intercellular communication. *Dev. Biol.* **204,** 80–96
25. Vainio, S., Heino, S., Mansson, J.-E., Fredman, P., Kuismanen, E., Vaarala, O., and Ikonen, E. (2002) Dynamic association of human insulin receptor with lipid rafts in cells lacking caveolae. *EMBO Rep.* **3,** 95–100
26. Manautou, J. E., de Waart, D. R., Kunne, C., Zelcer, N., Goedken, M., Borst, P., and Elferink, R. O. (2005) Altered disposition of acetaminophen in mice with a disruption of the Mrp3 gene. *Hepatology* **42,** 1091–1098
27. Oh, H.-J., Park, E.-S., Kang, S., Jo, I., and Jung, S.-C. (2004) Long-term enzymatic and phenotypic correction in the phenylketonuria mouse model by adeno-associated virus vector-mediated gene transfer. *Pediatr. Res.* **56,** 278–284
28. Jung, S.-C., Park, J.-W., Oh, H.-J., Choi, J.-O., Seo, K.-I., Park, E.-S., and Park, H.-Y. (2008) Protective effect of recombinant adeno-associated virus 2/8-mediated gene therapy from the maternal hyperphenylalaninemia in offsprings of a mouse model of phenylketonuria. *J. Korean Med. Sci.* **23,** 877–883
29. Gao, G.-P., Alvira, M. R., Wang, L., Calcedo, R., Johnston, J., and Wilson, J. M. (2002) Novel adeno-associated viruses from rhesus monkeys as vectors for human gene therapy. *Proc. Natl. Acad. Sci. U.S.A.* **99,** 11854–11859
30. Jung, S. C., Han, I. P., Limaye, A., Xu, R., Gelderman, M. P., Zerfas, P., Tirumalai, K., Murray, G. J., During, M. J., Brady, R. O., and Qasba, P. (2001) Adeno-associated viral vector-mediated gene transfer results in long-term enzymatic and functional correction in multiple organs of Fabry mice. *Proc. Natl. Acad. Sci. U.S.A.* **98,** 2676–2681
31. Cuenda, A. (2000) Mitogen-activated protein kinase kinase 4 (MKK4). *Int. J. Biochem. Cell Biol.* **32,** 581–587
32. Saito, C., Zwingmann, C., and Jaeschke, H. (2010) Novel mechanisms of protection against acetaminophen hepatotoxicity in mice by glutathione and *N*-acetylcysteine. *Hepatology* **51,** 246–254
33. Lang, C., Meier, Y., Stieger, B., Beuers, U., Lang, T., Kerb, R., Kullak-Ublick, G. A., Meier, P. J., and Pauli-Magnus, C. (2007) Mutations and polymorphisms in the bile salt export pump and the multidrug resistance protein 3 associated with drug-induced liver injury. *Pharmacogen. Genomics* **17,** 47–60
34. Aleksunes, L. M., Campion, S. N., Goedken, M. J., and Manautou, J. E. (2008) Acquired resistance to acetaminophen hepatotoxicity is associated with induction of multidrug resistance-associated protein 4 (Mrp4) in proliferating hepatocytes. *Toxicol. Sci.* **104,** 261–273
35. Aleksunes, L. M., Scheffer, G. L., Jakowski, A. B., Pruimboom-Brees, I. M., and Manautou, J. E. (2006) Coordinated expression of multidrug resistance-associated proteins (Mrps) in mouse liver during toxicant-induced injury. *Toxicol. Sci.* **89,** 370–379
36. Zamek-Gliszczynski, M. J., Nezasa, K., Tian, X., Bridges, A. S., Lee, K., Belinsky, M. G., Kruh, G. D., and Brouwer, K. L. (2006) Evaluation of the role of multidrug resistance-associated protein (Mrp) 3 and Mrp4 in hepatic basolateral excretion of sulfate and glucuronide metabolites of acetaminophen, 4-methylumbelliferone, and Harmol in Abcc3$^{-/-}$ and Abcc4$^{-/-}$ mice. *J. Pharmacol. Exp. Ther.* **319,** 1485–1491
37. Okuyama, H., Nakamura, H., Shimahara, Y., Araya, S., Kawada, N., Yamaoka, Y., and Yodoi, J. (2003) Overexpression of thioredoxin prevents acute hepatitis caused by thioacetamide or lipopolysaccharide in mice. *Hepatology* **37,** 1015–1025
38. Nakagawa, H., Maeda, S., Hikiba, Y., Ohmae, T., Shibata, W., Yanai, A., Sakamoto, K., Ogura, K., Noguchi, T., Karin, M., Ichijo, H., and Omata, M. (2008) Deletion of apoptosis signal-regulating kinase 1 attenuates acetaminophen-induced liver injury by inhibiting c-Jun N-terminal kinase activation. *Gastroenterology* **135,** 1311–1321
39. Maurel, M., and Rosenbaum, J. (2012) Closing the gap on drug-induced liver injury. *Hepatology* **56,** 781–783
40. Asamoto, M., Hokaiwado, N., Murasaki, T., and Shirai, T. (2004) Con-

nexin 32 dominant-negative mutant transgenic rats are resistant to hepatic damage by chemicals. *Hepatology* **40,** 205–210
41. Naiki-Ito, A., Asamoto, M., Naiki, T., Ogawa, K., Takahashi, S., Sato, S., and Shirai, T. (2010) Gap junction dysfunction reduces acetaminophen hepatotoxicity with impact on apoptotic signaling and connexin 43 protein induction in rat. *Toxicol. Pathol.* **38,** 280–286
42. Locke, D., Liu, J., and Harris, A. L. (2005) Lipid rafts prepared by different methods contain different connexin channels, but gap junctions are not lipid rafts. *Biochemistry* **44,** 13027–13042
43. Patel, S. J., King, K. R., Casali, M., and Yarmush, M. L. (2009) DNA-triggered innate immune responses are propagated by gap junction communication. *Proc. Natl. Acad. Sci. U.S.A.* **106,** 12867–12872
44. Simons, K., and Toomre, D. (2000) Lipid rafts and signal transduction. *Nat. Rev. Mol. Cell Biol.* **1,** 31–39
45. Fukuda, T., Ikejima, K., Hirose, M., Takei, Y., Watanabe, S., and Sato, N. (2000) Taurine preserves gap junctional intercellular communication in rat hepatocytes under oxidative stress. *J. Gastroenterol.* **35,** 361–368
46. Henderson, N. C., Pollock, K. J., Frew, J., Mackinnon, A. C., Flavell, R. A., Davis, R. J., Sethi, T., and Simpson, K. J. (2007) Critical role of c-jun (NH2) terminal kinase in paracetamol- induced acute liver failure. *Gut* **56,** 982–990
47. Teng, C.-H., Huang, W.-N., and Meng, T.-C. (2007) Several dual specificity phosphatases coordinate to control the magnitude and duration of JNK activation in signaling response to oxidative stress. *J. Biol. Chem.* **282,** 28395–28407